Research Article

Chunna Cui, Yuemei Sun, and Jitao Huang*

Separation of graphene oxides of different sizes by multi-layer dialysis and anti-friction and lubrication performance

https://doi.org/10.1515/gps-2023-0114
received June 27, 2023; accepted October 1, 2023

Abstract: As a 2D carbon material, graphene exhibits a unique structure and outstanding properties and has been widely applied in various fields. Because the properties of graphene are closely related to their structural parameters, graphene with different size distributions is suitable for different applications. However, current methods of fine-scale separation of graphene and its derivatives have certain limitations. In this study, graphene oxide (GO) size separation using multilayer dialysis was proposed. Multiple size separation in one step was achieved by customizing the dialysis size of each layer according to the actual requirements. In this way, GOs of different sizes were separated and large-scale synthesis can be achieved using this method. Meanwhile, the anti-friction and lubrication properties of aqueous dispersion solutions of GOs of different sizes were investigated. The results indicated significant improvements of the anti-friction and lubrication properties of GO samples prepared by the proposed method, as large-scale GOs can act as lubricants by relieving, if not preventing, friction between the two friction surfaces.

Keywords: separation, size distribution, graphene oxides, anti-friction and lubrication performance

1 Introduction

As an important nanomaterial, graphene and its oxides have a wide range of applications and have continuously attracted attention and been studied [1–4]. At present, research on the application of graphene has been widely distributed in heat conduction [5], electricity conduction [6], friction [7], composite materials [8], adsorption [9], and other aspects [10,11]. The size of graphene material has an important impact on its application performance, and the properties and application scenarios of different sizes of graphene are very different. Such as large size graphene is more suitable for the preparation of super fibers [12], high-performance absorbing graphene microflowers [13], etc. Graphene of small size is more suitable for use in the preparation of quantum dots [14], etc. In addition to differences in function, the effects on biodistribution are also different. Studies have shown that larger graphene oxide (GO) particles accumulate in the lung, and smaller GO particles are retained in the liver in mice [15]. There are still many differences in the properties of graphene of different sizes that need to be investigated.

Size separation of graphene, GO, and their derivatives has been a hot topic [16–19]. Indeed, some approaches of size separation of graphene and GO have been reported [20,21], including centrifugal separation [22,23], electrophoresis separation [24,25], filtration separation [26], pH-assisted separation [27], and others. However, these approaches have not been widely applied in the industry due to various limitations. Based on this, we propose the application of dialysis, a common washing and impurity removal approach, in the size separation of graphene.

The dialysis [28–32] is a separation and purification technology that separates small and large molecules based on the mechanism that small molecules can diffuse into water (or buffer) through semi-permeable membranes. As a physical process, the rationale of dialysis is the concentration difference of matters. Specifically, dialysis is dependent on semi-permeable membranes, which are literally refined sieves that allow only molecules with radii smaller than the mesh to pass through. Additionally, the dialysis process is a diffusion process, which is a result of Brownian movements of all molecules in the solution.

* **Corresponding author: Jitao Huang,** College of Chemistry and Materials Science, Fujian Normal University, 32 Shangsan Road, Fuzhou, Fujian 350007, China, e-mail: huangjitao818@126.com
Chunna Cui: College of Chemistry and Materials, Ningde Normal University, Ningde, Fujian 352100, China
Yuemei Sun: College of Chemistry and Materials Science, Fujian Normal University, 32 Shangsan Road, Fuzhou, Fujian 350007, China

Generally, dialysis bags or dialysis membranes are used in dialysis, and the molecular weight cutoff ranges from 100 to 1,000,000, indicating small mesh diameters. In this way, impurities in GO dispersion such as residual inorganic salts can be removed during GO preparation. Based on that, separation of GO of different sizes was achieved by dialysis of GO dispersion using membrane with different mesh diameters and this approach is promising for large-scale production. The proposed multi-layer dialysis set-up can realize separation of GO of different sizes in one step.

Owing to their unique quantum size effect and surface effect, nanoparticles exhibit unique properties that enable their applications in anti-friction and lubrication field [33,34]. As a novel nanomaterial with unique 2D structure, graphene is highly promising in applications of anti-friction and lubrication [35–37]. In this study, the prepared GOs were separated into GOs of three different sizes by dialysis and the effects of GO size on its anti-friction and lubrication performance were investigated.

2 Materials and methods

2.1 Preparation of GO

Graphite powder (2.0 g, mesh number = 325 mesh) was added into concentrated sulfuric acid (70 mL) in a 250 mL flask and mechanically stirred (200 rpm) in ice bath for 30 min, followed by slow addition of $KMnO_4$ (7.0 g) to keep the suspension temperature below 5°C. Then, the reaction system was transferred to water bath at 35°C and stirred (300 rpm) for 2 h, followed by addition of 200 mL water and 15 h stirring. After this, 5 mL of H_2O_2 (30%) was added to the reaction solution dropwise, resulting in a change in color from dark brown to yellow. The mixture was filtered and rinsed with 5% HCl solution (50 mL) three times to remove metallic ions, rinsed with water until neutral, and then filtered to obtain solid GO samples.

2.2 Separation of GO by multi-layer dialysis

The screen cloth was rinsed and semi-attached (relaxed with adjustable inter-layer distances) on a 50 L bucket by layers (mesh diameters of upper and lower layers were 18 and 6.5 μm, respectively). An air pump was arranged on each layer to generate bubbles and the solution was stirred to avoid sedimentation of GO. The bucket was filled with water, a 5 L dispersion of 5.0 g GO was added on the upper layer, and the air pump was turned on. After 48 h dialysis, solutions on different layers were extracted and filtered. Products on the upper layer were denoted as GO-L, products between the upper and lower layers were denoted as GO-M, and products below the lower layer were denoted as GO-S. The original GO was denoted as GO-O.

2.3 Tests of friction performance of GO

In order to have the dispersion stability of GO in pure water, a surfactant triethanolamine soap was used to modify the compatibility of water and GO. First, a certain proportion of surfactant and GO were added to pure water. Then the mixture was sonicated for 15 min, stirred in 50°C water bath for 30 min, and stored.

In this study, the friction wear performance of samples was evaluated by MS-10A four ball friction wear tester, while point contact and Grade II standard steel ball with a diameter of 12.7 mm were used. The key indicator of lubricant bearing capacity is the maximum non-seizure load (PB value), which is usually measured according to China GB/T3142-82. GO dispersions were tested under conditions of tester main axle rotation speed = 1,450 rpm, room temperature, and duration = 10 s. The samples were characterized by optical microscopy and the wear spot diameters of the three lower balls were measured. Optimized GO concentration range and friction performance of different samples were determined based on wear spot diameter (D value) and PB value. Long-term anti-wear tests were conducted according to SH/T0189-92 under conditions of load = 147 N, temperature = 75 ± 2°C, rotation speed of tester main axle = 1,200 rpm, and duration = 60 min. The wear resistance of the samples was evaluated based on the wear rate of the steel balls and the friction coefficients obtained.

3 Results and discussion

3.1 Rationale of size separation

Figure 1 illustrates the separation of GO by multi-layer dialysis. As observed, the separation process is indeed a diffusion process: GOs with small layer diameters in disperse phases diffuse from high concentration dispersion into low concentration dispersion mediums via the screen cloth until equilibrium of osmotic pressure. Owing to

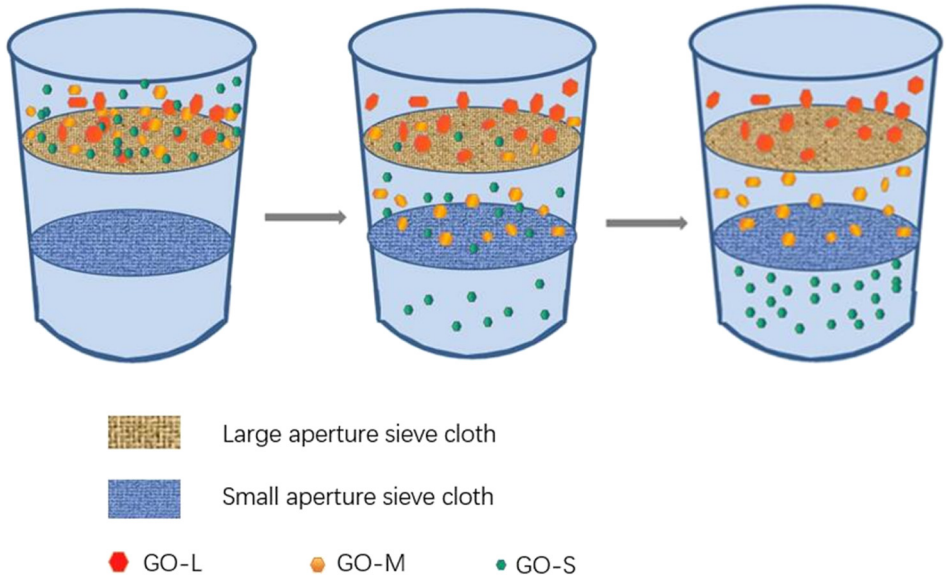

Figure 1: Schematic of dialysis separation of GOs.

selection by the mesh of screen cloth, GO with small layer diameters in dispersion can diffuse through, while GO with large layer diameters cannot. The multi-layer dialysis separation membrane was designed accordingly to achieve separation of GO of different sizes in one step.

The driving force of dialysis is the concentration difference. At early stage of dialysis, dialysis separation is fast and spontaneous as GO concentration in the upper layer was significantly higher than that in other layers. Once GOs diffused to the middle layer, GOs with large layer diameters were held in the upper layer. Then, GO with small layer diameters further diffused to the lower layer. All layers of screen cloth were semi-attached and the volumes between each two layers were adjustable. The concentration of solution was indicated by its color and the solution concentration was in descending order from the upper layer to the lower layer so that GOs with small layer diameters in the upper layer can diffuse to the lower layer while GOs with large layer diameters are held by the screen cloth, thus achieving separation of GOs of different layer diameters. Figure 2 illustrates the rationale of GO dialysis.

3.2 SEM of GOs and size distribution

Figure 3 shows SEM and size distribution of the GO samples. As observed, more than 87% of GO-L was in the 25–50 μm size range, more than 90% of GO-L was in the 10–25 μm size range, and more than 93% of GO-L was below 10 μm size range. The sizes of GOs on the upper layer were large and sizes of GOs on the lower layer were small. The size distribution of GO-O was in 0–60 μm. Through calculation, the average size of GO-L was 30.29 μm, the average size of GO-M was 15.85 μm, the average size of GO-S was 5.99 μm, and the average size of GO-O was 21.17 μm.

3.3 XRD and Raman spectrum

As shown in Figure 4 (XRD), peak positions were located at 10–13°, indicating that all samples obtained were GO. The XRD peak positions of GO-L, GO-M, and GO-S were at 2θ = 12.38°, 12.15°, and 12.09°, respectively, while that of the original sample was at 2θ = 12.11°. The full width at half maxima of GO-L, GO-M, and GO-S were 1.06°, 1.12°, and 1.18°, indicating that the disorder of GO is negative to its

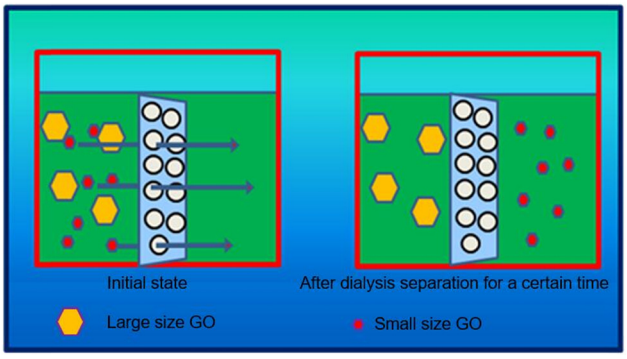

Figure 2: Rationale of dialysis separation of GOs.

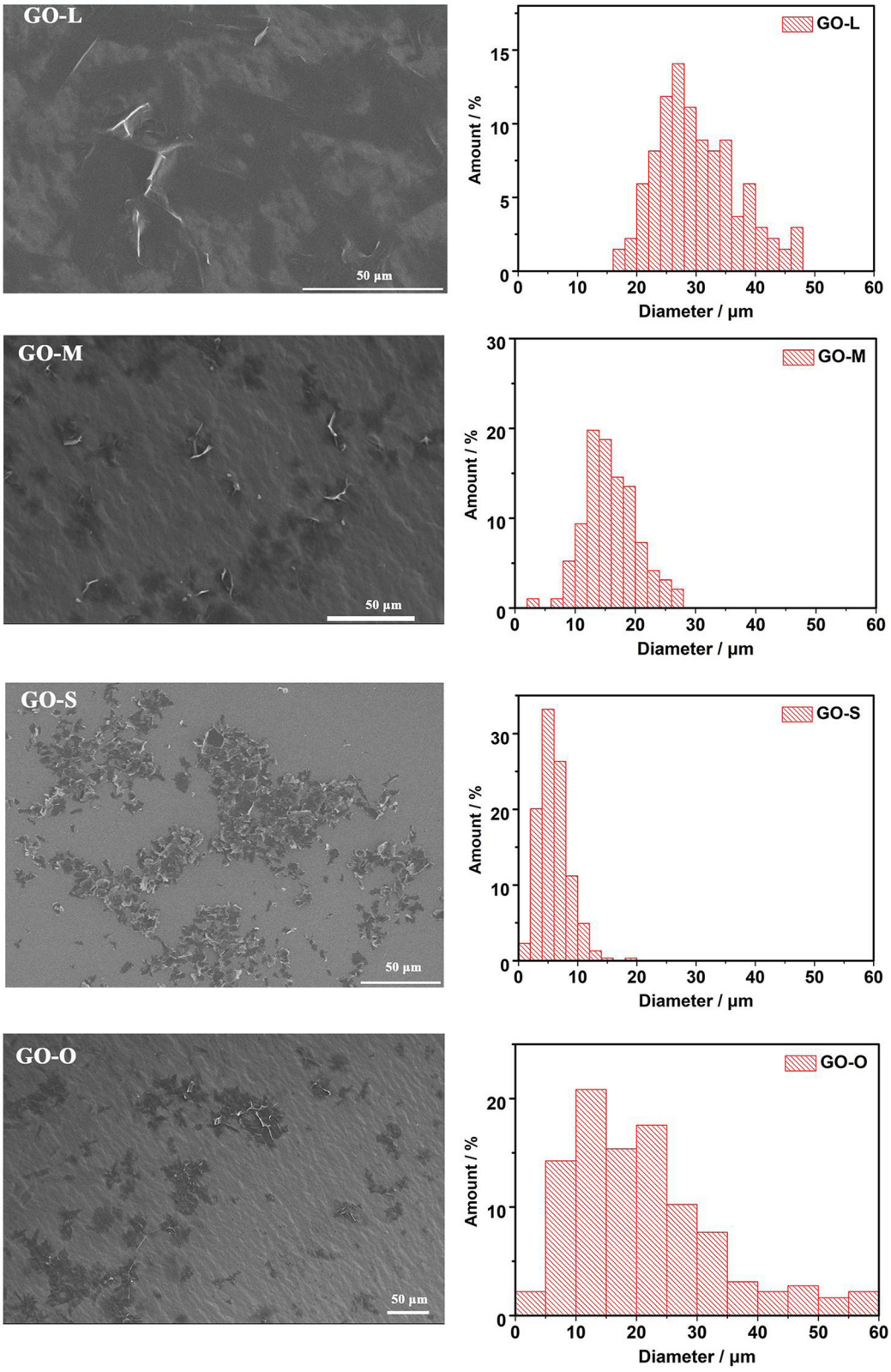

Figure 3: SEM and corresponding statistical graph of particle size distribution (Scale = 50 μm in SEM image. The statistical graph of particle size distribution of each sample is obtained by counting more than 1,000 pieces in the SEM diagram.).

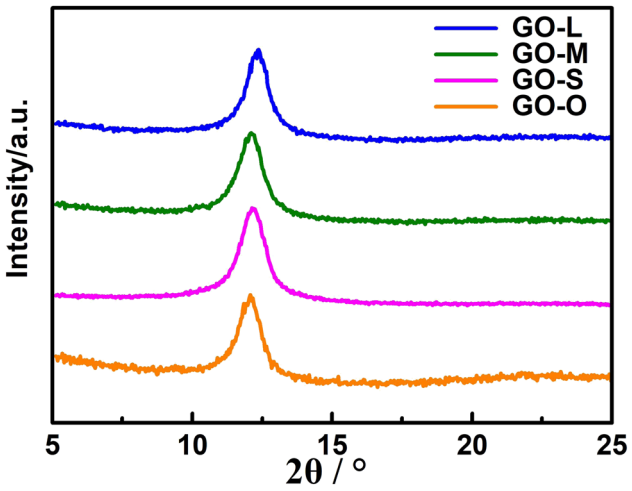

Figure 4: XRD patterns of different "dialysis" layers GO.

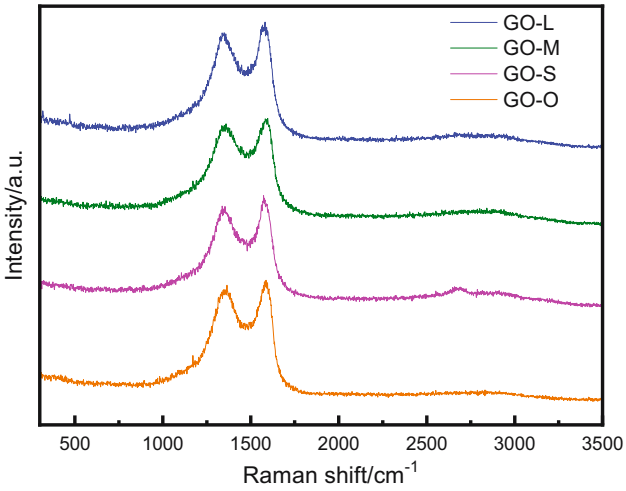

Figure 5: Raman spectrogram of different "dialysis" layers GO.

layer size. The grain size calculated by the Scherrer equation follows the descending order of GO-L, GO-M, GO-S, which is consistent with the SEM results.

The Raman spectrum of GO samples (Figure 5) illustrates defect-related peak positions D at 1,340–1,360 cm^{-1}, phonon E2g induced peak positions G at 1,575–1,595 cm^{-1}, and extremely weak peak positions 2D. Generally, the distance between the defects in graphene (LD) can be estimated by the intensity ratio of peak positions D and peak positions G (I_D/I_G). For GO, LD decreases and defect density increases as I_D/I_G decreases. I_D/I_G of GO-L, GO-M, and GO-S were 0.922, 0.909, and 0.890, respectively, while that of GO-O was 0.906. Hence, LD of GO-L, GO-M, and GO-S are in ascending order. This can be attributed to the increasing edge ratio induced by increasing concentration of GOs with small layer diameters. However, high defect intensity leads to small diameters of GO layers and increased ratio of defects and functional groups, which in turn results in severe edge damages. In other words, effective edges of GOs with small layer diameters decreased and peak positions D, which is originated from vibrations of graphite carbon crystalline edge, degraded. Hence, I_D/I_G decreased with the layer diameter of GO. In summary, Raman spectrum of GO samples indicated that the layer diameters of GO-L, GO-M, and GO-S are in descending order.

3.4 XPS spectrum

Figure 6 and Table S1 show the XPS spectra of GO-L, GO-M, GO-S, and GO-O. The C/O atomic ratio is a key indicator of oxidation of GO layers. Under constant conditions, the C/O ratio is positively related to layer diameter of GO. Hence, variation of the C/O ratio also reflects separation of GOs with different layer diameters. Figure 6(a) demonstrates that major elements of the samples obtained were carbon and oxygen. The C/O ratio of GO-L, GO-M, GO-S, and GO-O were 1.983, 1.781, 1.662, and 1.761, respectively. A possible reason is that edge intensity is negatively related to the layer diameter, while oxidation of GO occurs at edges.

The C 1s XPS spectrum of GO consists of three carbon bonds: C–C/C═C (284.6 eV), C–O (286.6–286.9 eV), and C═O (288.4–289 eV). Table S1 summarizes the percentages of different carbon bonds. The contents of C–C bonds in GO-L, GO-M, and GO-S were 0.40, 0.34, and 0.26, respectively; the content of C–C bond is negatively related to GO oxidation. The contents of C═O bonds in GO-L, GO-M, and GO-S were 0.10, 0.11, and 0.30, respectively; the content of C═O bond is positively related to GO oxidation. In summary, oxidations of GO-L, GO-M, and GO-S are in ascending order.

Similarly, trend of the peak intensity ratio of non-oxidized carbon atoms (C–C/C═C) and oxidized ones (C–O, C═O and O–C═O) can be determined based on the peak split of XPS (Figure 6(b)–(e)). The peak intensity ratio of oxidized carbon atoms of GO-L, GO-M, and GO-S is in ascending order, while that of GO-O is neither highest nor lowest. In other words, the layer diameter of GO-L, GO-M, and GO-S is in descending order.

3.5 Friction performance of GO aqueous dispersion solution

Figure 7 shows the anti-friction performance of GO as lubricant and the effects of its concentration. As shown in Figure 7(a), the PB value fluctuated slightly with the

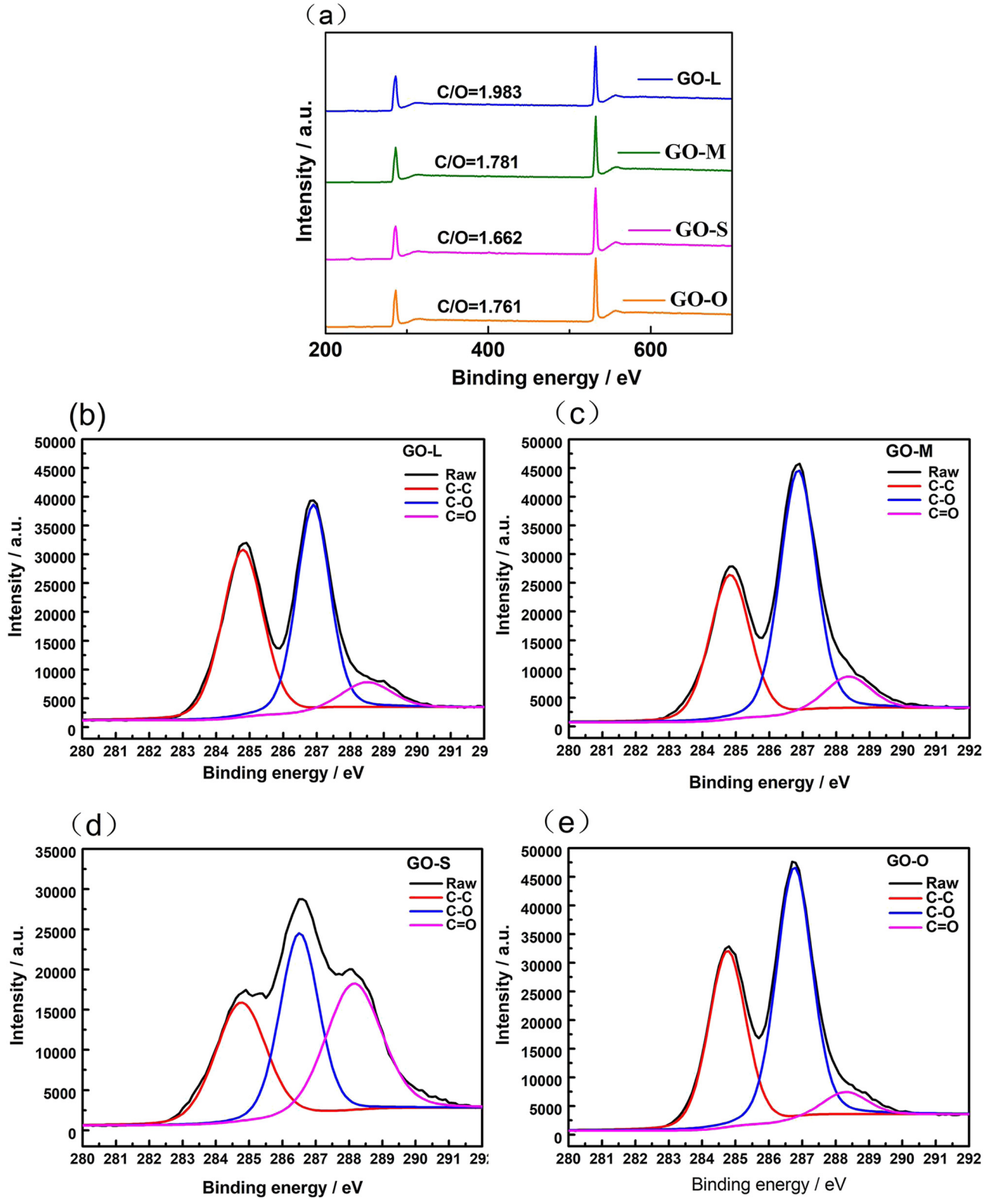

Figure 6: XPS spectra: (a) original spectra, (b)–(e) are the C1s sub-peaks of GO-L, GO-M, GO-S, and GO-O, respectively.

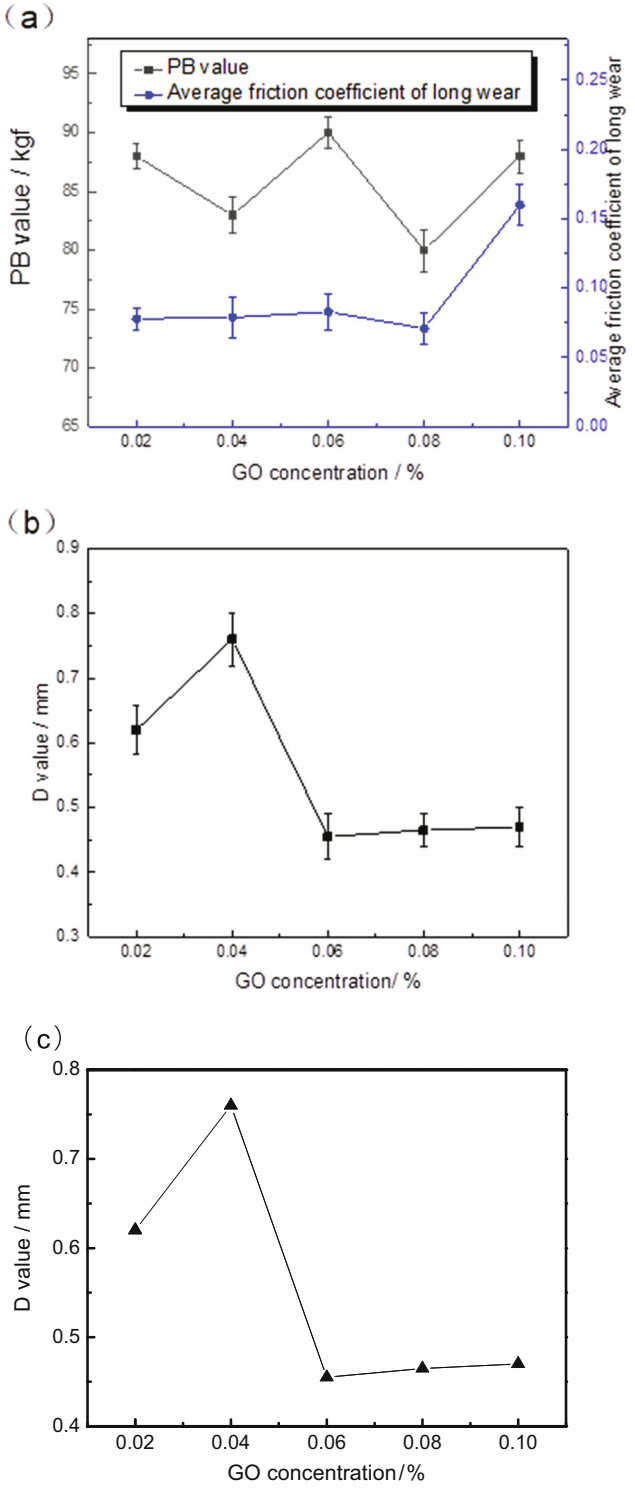

Figure 7: (a) Effect of GO addition concentration and as a lubricating additive on PB value and average friction coefficient of long grinding and (b) effect of GO addition concentration and as a lubricating additive on *D* value.

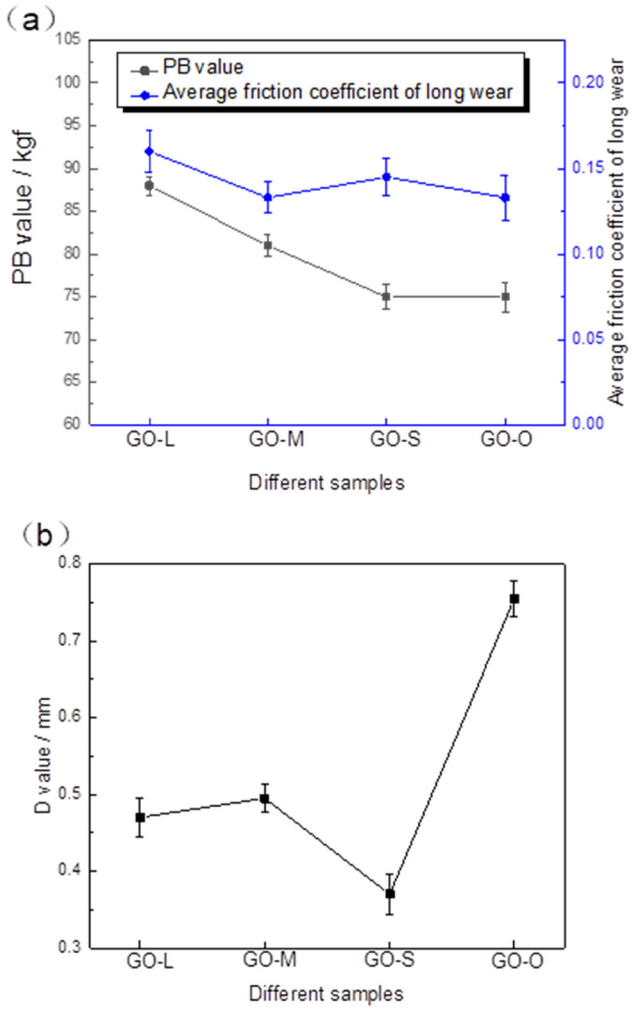

Figure 8: (a) Effect of GO lubricating additive of different particle sizes on PB value and average friction coefficient of long grinding and (b) effect of GO lubricating additive of different particle sizes on *D* value.

GO concentration and the optimized concentration was 0.06%. The maximum PB value obtained was 90 kgf. Indeed, long-term average friction coefficient increased significantly once the GO concentration exceeds 0.08%, which indicates good friction reduction performance at GO concentration below 0.08%. The *D* value at GO concentration above 0.06% was significantly lower than that at GO concentration below 0.06. Based on friction reduction performance and cost, 0.06% is supposed as the optimized GO concentration.

GO size is a key factor for lubricant friction performance as layer diameter may affect motion of GO layers during motion of lubricant: GOs with small layer diameters can easily move, while GOs with large layer diameters may induce resistances and expand the contact friction surface, resulting in good lubrication performance. The average particle sizes of GO-L, GO-M, GO-S, and GO-O were approximately 30, 16, 6, and 21 μm, respectively. Also, the PB values, long mill average friction coefficients, and *D* values of these samples were determined.

As observed in Figure 8, the PB value of GO decreased with its average particle size. Meanwhile, the PB value decreased and the *D* value increased as the size distribution range of GO samples increased, demonstrating significant effects of GO size on friction performance of lubricants. As the GO size increased, GOs with large layer diameters were decelerated under tractions owing to large layer diameter and contact area of the two friction surfaces of lubricant so that the two friction surfaces are effectively separated, while GOs with small layer diameters in metallic friction surface do not favor protective film, resulting in lower PB value, but smaller *D* value.

The higher the PB value the better the lubrication performance of the mixture. Smaller *D* values indicate better lubricity and more energy savings. Smaller values of *D* indicate that the force is more uniform, and the wear resistance and continuity of the mixture are better. Comparative analysis of PB and *D* values shows that GO with a narrower size distribution after dialysis separation, especially GO-L, has better friction lubrication performance than GO samples before separation.

4 Conclusions

We designed a new method to separate GO using cloth sieves with different pore sizes. GO samples with different diameters can be obtained simultaneously by multilayer dialysis and are characterized and tested. Specifically, GO separation was achieved by dialysis of screen cloth based on different GO layer diameters and differences in penetration speed and particle size allowed by screen cloth with different mesh diameters. The results showed that this approach is facile yet effective. The average size of GO-L is 30.29 μm intercepted by the macroporous sieve, and the average size of GO-S through the small hole screen is 5.99 μm. In addition, the anti-friction and lubrication properties of GOs of different particle sizes were investigated. The anti-friction and lubrication properties of GO aqueous dispersion solution obtained by this method were excellent, especially GO-L. As their sizes increased, GOs were decelerated under traction. For GO-L, the two friction surfaces can be effectively separated due to the large layer diameters and large contact area of the two friction surfaces of the lubricant.

Funding information: This work was financially supported by the Research funding project of Ningde Normal University (2019ZDK16, 2020Y04, and 2022T10), Fujian Science and Technology Department (2023Y0038 and 2021H0062), and the 2022 Ningde industry-university-research cooperation project (2022C001).

Author contributions: Chunna Cui: writing – original draft, writing – review and editing, methodology, and formal analysis; Yuemei Sun: formal analysis, visualization, and project administration; Jitao Huang: writing – original draft, project administration, and resources.

Conflict of interest: Authors state no conflict of interest.

Data availability statement: The datasets generated during and/or analyzed during the current study are available from the corresponding author on reasonable request.

References

[1] Novoselov KS, Geim AK, Morozov SV, Jiang D, Zhang Y, Dubonos SV, et al. Electric field effect in atomically thin carbon films. Science. 2004;306(5696):666–9. doi: 10.1126/science.1102896.

[2] Coroş M, Pogăcean F, Măgeruşan L, Socaci C, Pruneanu S. A brief overview on synthesis and applications of graphene and graphene-based nanomaterials. Front Mater Sci. 2019;13(1):23–32. doi: 10.1007/s11706-019-0452-5.

[3] Kumar N, Salehiyan R, Chauke V, Joseph Botlhoko O, Setshedi K, Scriba M, et al. Top-down synthesis of graphene: a comprehensive review. FlatChem. 2021;27(100224):2452–627. doi: 10.1016/j.flatc.2021.100224.

[4] Li X, Colombo L, Ruoff RS. Synthesis of graphene films on copper foils by chemical vapor deposition. Adv Mater. 2016;28(29):6247–52. doi: 10.1002/adma.201504760.

[5] Alam SN, Sharma N, Kumar L. Synthesis of graphene oxide (GO) by modified Hummers method and its thermal reduction to obtain reduced graphene oxide (rGO). GR. 2017;6(1):1–18. doi: 10.1016/j.matpr.2020.09.294.

[6] Francesco B, Luigi C, Guihua Y, Meryl S, Valentina T, Andrea CF, et al. 2D materials. graphene, related two-dimensional crystals, and hybrid systems for energy conversion and storage. Science. 2015;347(6217):1246501. doi: 10.1126/science.1246501.

[7] Dwivedi N, Patra T, Lee J, Yeo B, Srinivasan RJ, Dutta S, et al. Slippery and wear-resistant surfaces enabled by interface engineered graphene. Nano Lett. 2020;20(2):905–17. doi: 10.1021/acs.nanolett.9b03650.

[8] Razaq A, Bibi F, Zheng X, Papadakis R, Jafri S, Li H. Review on graphene–graphene oxide reduced graphene oxide-based flexible composites: from fabrication to applications. Materials (Basel). 2022;15(3):1012. doi: 10.3390/ma15031012.

[9] Yin M, Pan Y, Pan C. Adsorption properties of graphite oxide for Rhodamine B. Micro Nano Lett. 2019;14(11):1192–7. doi: 10.1049/mnl.2018.5820.

[10] Díaz EC, Martínez SB, Valcárcel. M. Rapid and simple nanosensor by combination of graphene quantum dots and enzymatic inhibition mechanisms. Sens Actuators B Chem. 2017;240:90–9. doi: 10.1016/j.snb.2016.08.153.

[11] Zhen X, Haiyan S, Xiaoli Z, Chao G. Ultra-strong fibers assembled from giant graphene oxide sheets. Adv Mater. 2013;25(2):188–93. doi: 10.1002/adma.201.

[12] Zhen X, Yingjun L, Xiaoli Z, Li P, Haiyan S, Yang X, et al. Ultrastiff and strong graphene fibers via full-scale synergetic defect engineering. Adv Mater. 2016;28:6449–56. doi: 10.1002/adma.201506426.
[13] Chen C, Jiabin X, Erzhen Z, Li P, Zichen C, Chao G. Porous graphene microflowers for high-performance microwave absorption. Nano-Micro Lett. 2018;10:26. doi: org/10.1007/s40820-017-0179-8.
[14] Jinli Z, Yanfeng T, Gang W, Jiarong M, Zhiduo L, Tongming S, et al. Green, rapid, and universal preparation approach of graphene quantum dots under ultraviolet irradiation. ACS Appl Mater Interfaces. 2017;9:14470–7. doi: 10.1021/acsami.6b11525.
[15] Liu JH, Yang ST, Wang HF, Chang YL, Cao AN, Liu YF. Effect of size and dose on the biodistribution of graphene oxide in mice. Nanomedicine (London). 2012;7(12):1801–12. doi: 10.2217/nnm.12.60.
[16] Amir K, Farzin R, Sasan N, Paul S. Molecular insights on the CH_4/CO_2 separation in nanoporous graphene and graphene oxide separation platforms: adsorbents versus membranes. Phys Chem. 2017;121:12308–20. doi: 10.1021/acs.jpcc.7b03728J.
[17] Ruirui H, Yijia H, Meirong H, Guoke Z, Hongwei Z. Strong adhesion of graphene oxide coating on polymer separation membranes. Langmuir. 2018;34:10569–79. doi: 10.1021/acs.langmuir.8b02342.
[18] Chao X, Jing H, Xin P, Yuting Z, Jing H, Rong H, et al. Tunable graphene oxide nanofiltration membrane for effective dye/salt separation and desalination. ACS Appl Mater Interfaces. 2021;13(46):55339–48. doi: 10.1021/acsami.1c16141.
[19] Jitao H, Chunna C, Xiaomin Z, Guohua C. Size separation of graphene oxide via multi-layer filtering by silica gel column. Mater Express. 2019;9(9):1025–32. doi: 10.1166/mex.2019.1591.
[20] Yong L, Dong Z, Shiwu P, Yanyun L, Yu S. Size separation of graphene oxide using preparative free-flow electrophoresis. J Sep Sci. 2015;38:157–63. doi: 10.1002/jssc.20140.
[21] Martin P. Nanomaterials meet microfluidics. Chem Commun. 2011;47(20):5671–80. doi: 10.1039/c1cc11060h.
[22] Xiaoming S, Dachao L, Junfeng L, David GE. Monodisperse chemically modified graphene obtained by density gradient ultra-centrifugal rate separation. ACS Nano. 2010;4(6):3381–9. doi: 10.1021/nn1000386.
[23] Alexander AG, Mark CH. Solution phase production of graphene with controlled thickness via density differentiation. Nano Lett. 2009;9(12):4031–6. doi: 10.1021/nl902200b.
[24] Jingjing Z, Guifen C, Wei Z, Peng L, Lei W, Qiaoli Y, et al. High-resolution separation of graphene oxide by capillary electrophoresis. Anal Chem. 2011;83(23):9100–6. doi: 10.1021/ac202136n.
[25] Cui C, Huang J, Huang J, Chen G. Size separation of mechanically exfoliated graphene sheets by electrophoresis. Electrochim Acta. 2017;258(20):793–9. doi: 10.1016/j.electacta.2017.11.128.
[26] Ji C, Yingru L, Liang H, Naer J, Chun L, Gaoquan S. Size fractionation of graphene oxide sheets via filtration through track-etched membranes. Adv Mater. 2015;27:3654–60. doi: 10.1002/adma.201.
[27] Xiluan W, Hua B, Gaoquan S. Size fractionation of graphene oxide sheets by pH-assisted selective sedimentation. Am Chem Soc. 2011;133:6338–42. doi: 10.1021/ja200218y.
[28] Eswari JS, Naik S. A critical analysis on various technologies and functionalized materials for manufacturing dialysis membranes. Mater Sci Technol. 2020;3:116–26. doi: 10.1016/j.mset.2019.10.011.
[29] Fujioka T, Boivin S. Dialysis as a new pre-treatment technique for online bacterial counting. Sci Total Environ. 2020;714(3):136768. doi: 10.1016/j.scitotenv.2020.136768.
[30] Mollahosseini A, Abdelrasoul A, Shoker A. Latest advances in zwitterionic structures modified dialysis membranes. Mater Today Chem. 2020;15:100227. doi: 10.1016/j.mtchem.2019.100227.
[31] Davenport A. New dialysis technology and biocompatible materials. Contrib Nephrol. 2017;189:130–6. doi: 10.1159/000450739.
[32] Westphalen H, Saadati S, Eduok U, Abdelrasoul A, Shoker A, Choi P. Case studies of clinical hemodialysis membranes: influences of membrane morphology and biocompatibility on uremic blood-membrane interactions and inflammatory biomarkers. Sci Rep. 2020;10(1):14808. doi: 10.1038/s41598-020-71755-8.
[33] Yang H, Yilmaz G, Han G, Eriten M, Zhang Z, Yu S. A quick response and tribologically durable graphene heater for rapid heat cycle molding and its applications in injection molding. Appl Therm Eng. 2020;167:114791. doi: 10.1016/j.applthermaleng.2019.114791.
[34] Huang Z, Xue P, Chen C, Diao D. Rapid fabrication of ultra-wear-resistant graphene nanocrystallite film by direct laser writing. Appl Surf Sci. 2022;604:154658. doi: 10.1016/j.apsusc.2022.154658.
[35] Shahin M, Munir K, Wen C, Li Y. Nano-tribological behavior of graphene nanoplatelet reinforced magnesium matrix nanocomposites. JMA. 2021;9(3):895–909. doi: 10.1016/j.jma.2020.10.001.
[36] Wang H, Zhang H, Zhang J, Zhao Y. Improving tribological performance of fluoroether rubber composites by ionic liquid modified graphene. Compos Sci Technol. 2019;170:109–15. doi: 10.1016/j.compscitech.2018.11.041.
[37] Zhao J, Huang Y, Li Y, Gao T, Dou Z, Mao J, et al. Superhigh-exfoliation graphene with a unique two-dimensional (2D) microstructure for lubrication application. Appl Surf Sci. 2020;513:145608. doi: 10.1016/j.apsusc.2020.145608.